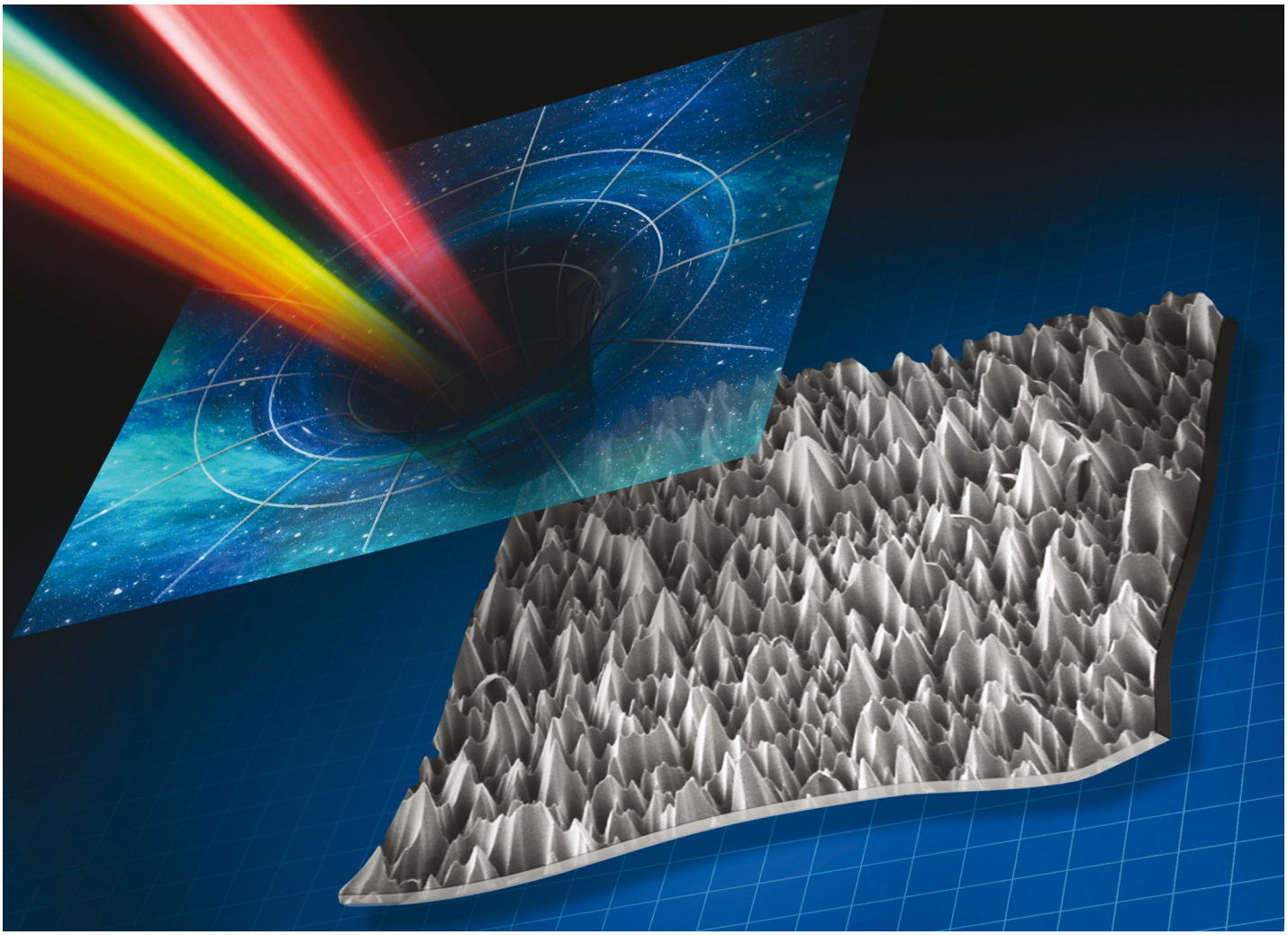

Showcasing research from National Metrology Institute of Japan (NMIJ) at National Institute of Advanced Industrial Science and Technology (AIST), Japan, and Takasaki Advanced Radiation Research Institute at National Institutes for Quantum and Radiological Science and Technology (QST), Japan

Perfect blackbody sheets from nano-precision microtextured elastomers for light and thermal radiation management

Microtextured polydimethylsiloxane sheets work like 'black holes' for the radiation in the entire thermal infrared region while maintaining their flexibility and high resilience. Furthermore, pre-addition of carbon black can make the sheets visually perfect black as well.

As featured in:

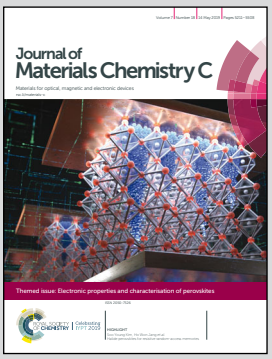

See Kuniaki Amemiya *et al.*, *J. Mater. Chem. C*, 2019, **7**, 5418.

ROYAL SOCIETY OF CHEMISTRY | Celebrating IYPT 2019

rsc.li/materials-c

Journal of Materials Chemistry C

PAPER

View Article Online
View Journal | View Issue

Cite this: J. Mater. Chem. C, 2019, 7, 5418

Perfect blackbody sheets from nano-precision microtextured elastomers for light and thermal radiation management†

Kuniaki Amemiya, *[a] Hiroshi Koshikawa,[b] Masatoshi Imbe,[a] Tetsuya Yamaki[b] and Hiroshi Shitomi[a]

Received 28th December 2018,
Accepted 5th April 2019

DOI: 10.1039/c8tc06593d

rsc.li/materials-c

Planar near-perfect blackbodies have wide applications ranging from dark-level reduction to light harvesting. Among them, carbon nanotube (CNT) forests have an unmatched mid-infrared blackbody performance, which is favourable for thermal radiation management. However, their inherent fragility against direct contact limits their broader use. Here we present a class of perfect blackbody sheets from elastomers outperforming CNT forests. Nano-precision micro-cavity arrays embossed on a polydimethylsiloxane (PDMS) sheet exhibit an exceptionally low reflectance of $\lesssim$0.0005 (an absorptance of $\gtrsim$0.9995) over the entire mid-infrared wavelengths (6–15 μm). In addition, this sheet maintains high resilience to tape-pulling, repeated bending, and scratching. The key technology is swift (>200 MeV) heavy ion manufacturing, yielding a highly flawless template of conical micro-cavities having necessary and sufficient openings (a dozen μm) and depths (several tens of μm) to trap ultrabroadband photons: this template affords scalable replication into PDMS blackbody sheets. Notably, the just-embossed PDMS sheets are visibly transmissive, whereas pre-addition of carbon black can extend the spectral range of near-perfect absorption as wide as from ultraviolet to mid-infrared wavelengths. Our tough and flexible planar blackbodies offer versatile applications of perfect absorbers/radiators, particularly with respect to thermal infrared management.

Introduction

A blackbody is a perfect absorber as well as an ideal radiator, obeying Planck's law, conventionally realized with a hole on a large cavity. Over the past decade, nanophotonic technologies have achieved a number of 'planar' near-perfect blackbodies,[1–5] enabling stray light baffling,[6,7] thermal radiators,[6–10] infrared detection,[11,12] solar energy harvesting[13–17] including for water desalination[18–20] or photocatalysis.[21] In particular, a planer blackbody valid for mid-infrared wavelengths is becoming a key component for thermal infrared management. For example, thermal imager optics use stray mid-infrared reducers (absorbers) and/or planar blackbody calibrators to achieve clear and accurate radiation temperature mapping.[6,7,22–25] A selective thermal blackbody is also in pressing need for passive radiative cooling.[8–10,26,27] For such applications, a planar blackbody should desirably have a reflectance of $\lesssim$0.001 (a typical criterion of whether it is a 'perfect' blackbody or not[28]) and high durability for field use as well.

Many of the recent 'planar' blackbodies rely on nanophotonic surface morphology: porosity and optical thickness (Fig. 1a and b). Porosity makes the effective refractive index, n_{eff}, close to unity[28] on the outermost surface, minimizing Fresnel reflection, $R = (n_{\mathrm{eff}} - 1)^2/(n_{\mathrm{eff}} + 1)^2$, and maximizing photo-absorption along with substantial optical thickness. Among pre-existing materials, only sparse forests of long-fibre (>tens of μm) carbon nanotube (CNT) meet these criteria to achieve unmatched low reflectance (<0.001 in the best case) over a wide spectral range from visible to mid-infrared wavelengths (0.4–15 μm).[2,11,29] Other nano-porous antireflective materials, such as moth-eye black silicon,[1,16] are typically incompatible for the mid-infrared, mainly owing to the limitation of manufacturable pore size and precision or insufficient optical thickness. Plasmonic or metamaterial perfect absorbers, although extensively studied,[30] generally show resonance and are rather suitable for filters or sensors.[31,32] Exceptionally, porous gold

[a] National Metrology Institute of Japan (NMIJ), National Institute of Advanced Industrial Science and Technology (AIST), 1-1-1 Umezono, Tsukuba, Ibaraki 305-8563, Japan. E-mail: k.amemiya@aist.go.jp
[b] Takasaki Advanced Radiation Research Institute, National Institutes for Quantum and Radiological Science and Technology (QST), 1233 Watanuki, Takasaki, Gunma, 370-1292, Japan

† Electronic supplementary information (ESI) available: Finite differential time domain simulation, optical characterization, measurement uncertainty and validation, fabrication of nickel metal replica, restoring the collapsed micro-cavities, thermal shock test, Fig. S1–S4 and Table S1. See DOI: 10.1039/c8tc06593d

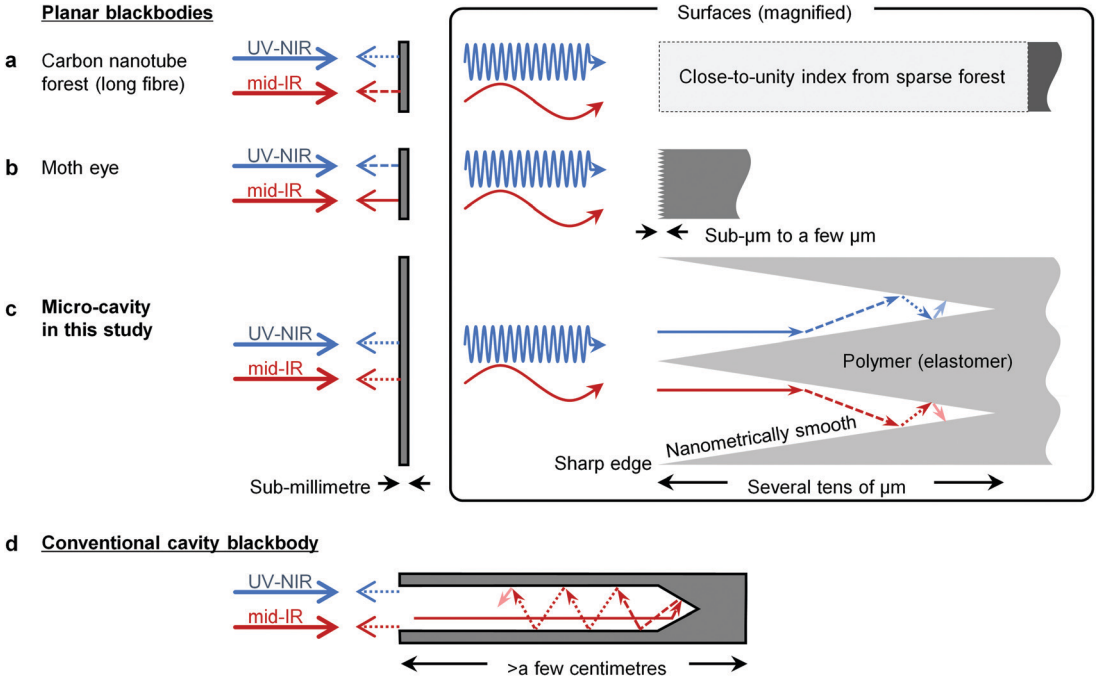

Fig. 1 Mechanisms of 'planar' blackbodies. (a) Long-fibre CNT forest. The sparse forest provides a close-to-unity index, suppressing Fresnel reflection over ultra-broadband photons while causing fragility. (b) Moth-eye. Sub-μm to a-few-μm surface texture provides a graded index reducing Fresnel reflection, while incompatible with much longer wavelength photons. (c) Micro-cavity array proposed here. High-aspect ratio of more than 5, and opening mouth on par with the longest wavelength of interest offer broadband perfect antireflection *via* multiple ray-optical bounces; the mechanism is similar to (d) a conventional cylindrical cavity blackbody, while nanometrically smooth surface and sharp edge of the micro-cavity are necessary to avoid diffusive escape of shorter wavelength photons. UV, ultraviolet; NIR, near-infrared; mid-IR, mid-infrared.

nano-dendrites exhibit broadband plasmonic absorption up to the mid-infrared,[12,18] whereas the absorptance is inferior to CNT forests. Meanwhile, the main disadvantage of porous blackbodies is insufficient mechanical strength. Although, even under vibration or shock the CNT forests are kept mounted on the substrate,[7] direct contact easily degrades their morphology, resulting in increased reflectance. Thus, a planar, truly perfect blackbody ($\lesssim$0.001 reflectance) of both mid-infrared compatibility and field-use durability has been unattained despite the emerging requirements for thermal radiation management.

To this end, we focused renewed attention on the strategy inspired by conventional cavity blackbodies (Fig. 1c and d). Graphite cavities of high aspect ratio (fraction of cavity depth to pore radius) can trap incident photons by multiple bounces and exhibit close-unity absorptance ($>$0.9995)[33] at broadband wavelengths, including the mid-infrared (Fig. 1d). This absorptance is still superior to that of most CNT forests.[7,28] Further, the cavity structure is much tougher than sparse nanotube arrays. However, the conventional cavities have non-planar geometry. An approach to turn this bulky blackbody into a sheet is planar arraying of 'microscopic' cavities (Fig. 1c). Therein, each high-aspect-ratio micro-cavity, fabricated on a photo-absorptive sheet, needs to have the opening on par with the longest wavelength of interest,[34,35] and, based on this ray-optical requirement, the micro-cavity is antireflective at all wavelengths shorter than the opening. Nano-photonic patterns are not absolutely necessary for perfect absorption. Instead, to ensure the ideal ray-optical behaviour without diffusive photon escape,[33] the micro-cavities need to have nanometrically smooth walls and sharp edges. In this respect, earlier attempts of micro-cavities such as black anodization[6] and lithographic photonic crystal[8] were unsatisfactory to achieve a truly perfect blackbody ($\lesssim$0.001 reflectance) for the mid-infrared.

In this study, we addressed the issue by simple two-step procedures of swift (high-energy) heavy ion fabrication[36] and replica moulding,[15,37–40] which can provide nano-precision micro-cavity arrays on a polydimethylsiloxane (PDMS) sheet. This microtextured elastomer sheet exhibited an exceptionally low reflectance ($\lesssim$0.0005) over the entire mid-infrared range (6–15 μm), while maintaining high mechanical resilience. This promising blackbody sheet affords the unprecedented management of light and thermal radiation.

Results and discussion

Fig. 2a–e shows our micro-cavities developed on poly ally diglycol carbonate (CR-39, in trade name) polymer substrate *via* swift heavy ion manufacturing (see Experimental section in details). This microtextured substrate is intended to be used as a template in the subsequent replica moulding process. The micro-cavities had sharp edges of well below 1 μm and smooth surfaces (Fig. 2d). The surface roughness is expected to be single-digit nanometres, as previously studied by atomic force

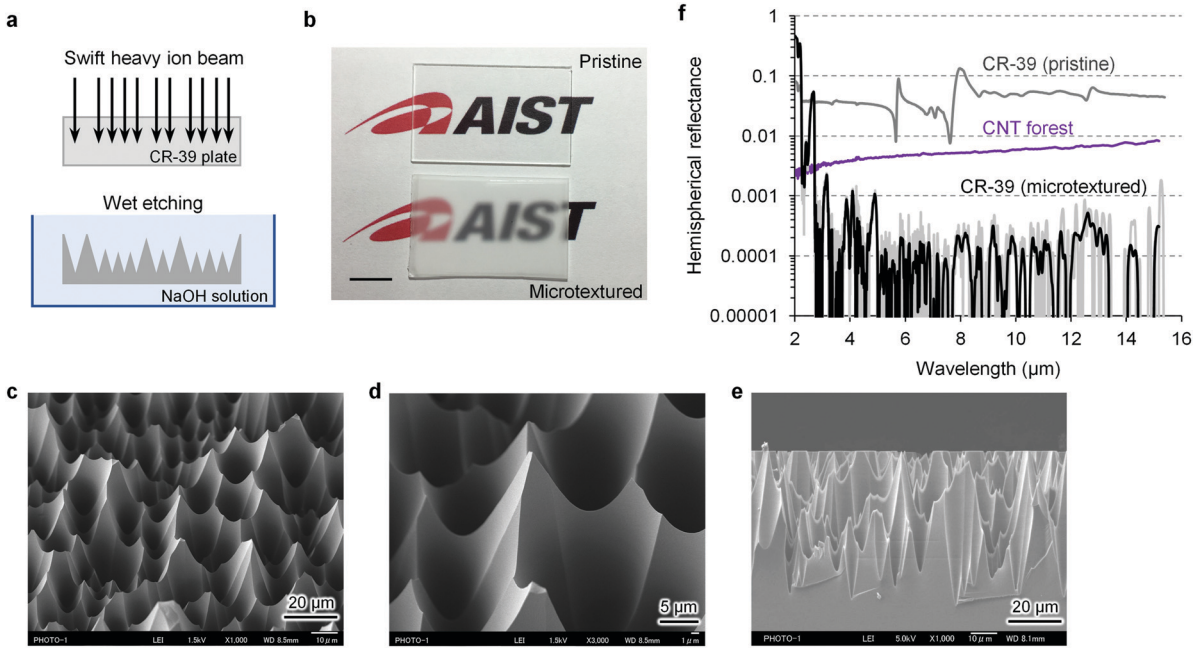

Fig. 2 Micro-cavity blackbody mould *via* swift heavy ion fabrication. (a) Fabrication processes. (b) Photograph for a pristine and a microtextured CR-39 plastic substrate. Scale bar, 10 mm. (c–e) SEM images of the micro-cavities textured on the CR-39 substrate: bird view (c and d) cross-section (e). (f) The mid-infrared hemispherical reflectance of the textured CR-39, in comparison with the Fresnel reflectance of a pristine CR-39 plate. The black solid line for the microtextured CR-39 denotes moving average of 20 neighbouring plots of the acquired data to show the trend buried in the noise level. Purple line denotes the results for a 40 μm-long multiwall CNT forest for comparison.

microscopy of an etched CR-39 substrate.[41] Each cavity opening diameter was over ten μm in average, and therefore compatible up to the mid-infrared. The cavity aspect ratio was more than 5, determined by the cross-section image of the micro-cavities' slopes (Fig. 2e). This aspect ratio was large enough to achieve an ultralow reflectance of <0.001,[34,35] as numerical simulation also predicted (Fig. S1, ESI†). Polymer or elastomer is a good choice for a base material because of not only high durability or resilience but also high infrared absorptivity attributable to many molecular vibration modes. The microtextured CR-39 substrate was visibly transmissive with a little haze, similar to frosted glass (Fig. 2b). Nevertheless, careful Fourier-transform infrared (FTIR) spectroscopy (see Experimental section, ESI† and Fig. S2a, b) confirmed that the as-microtextured CR-39 substrate was already the nearest-ever perfect blackbody ($\lesssim 0.0005$ reflectance) in entire mid-infrared wavelengths of 5–15 μm (Fig. 2f); this mid-infrared reflectance was as much as an order of magnitude lower than typical CNT forests.[7] Counterintuitively, the spectral reflectance had almost no specific peaks or dips; indeed, a pristine CR-39 plate showed extraordinary dispersion (Fig. 2f). The nanometrically precise micro-cavities were, thus, surprisingly effective for perfect absorption along with substantial optical thickness (physically <1 mm).

To make such precision textures of several-tens μm in depth, current standard micro-processes, including lithography[42] or machining,[43] may face difficulties; in the present study, we found that swift heavy ion manufacturing[36] allowed this hard-to-work fabrication. Bombardment of swift heavy ions on a polymer substrate and the following wet etching produce aperiodically-arrayed conical etch pits (see Experimental section, Fig. 2a). Each swift heavy ion degrades the polymer chain locally within a few nanometres along its trajectory,[39,44,45] leading to preferential nano-track etching. Importantly, a high-grade CR-39 polymer is homogeneously amorphous,[46] offering highly isotropic bulk erosion, even under long-time etching.[41] Consequently, we obtained the flawless micro-etch pits of nanometrically smooth walls and sharp edges, which can be hardly achieved with other polymer sheets.[39,45] Ion exposure density and etching time determine the pit opening diameters, while the appropriate choice of ion species (neon ions or heavier) and accelerated energy (>200 MeV) yields the desired pit aspect ratio (>5).[47] In the current situation of the ion beam irradiation chamber we used, a substrate of 100 mm × 100 mm size can be processed (a custom sample scanner would enable larger area fabrication).

Further, the microtextured CR-39 substrates were rigid but not brittle and, therefore, suitable for replica moulding[15,37–40] (see Experimental section, Fig. 3a). The replication process affords to massively emboss elastomer sheets, which more than compensates for the limited availability of a high energy ion beam facility (a cyclotron accelerator). The replica from PDMS had the precision spike texture (negative replica of the pit) of the smooth surface and the sharp tip (Fig. 3b), similar to the CR-39 master mould. Accordingly, the reflectance of the PDMS replica was <0.001 over the almost entire wavelengths of 6–15 μm (Fig. 3e). At some wavelengths (~ 9, 10 and 12.5 μm), the reflectance was 0.001–0.002. Nevertheless, it was comparable

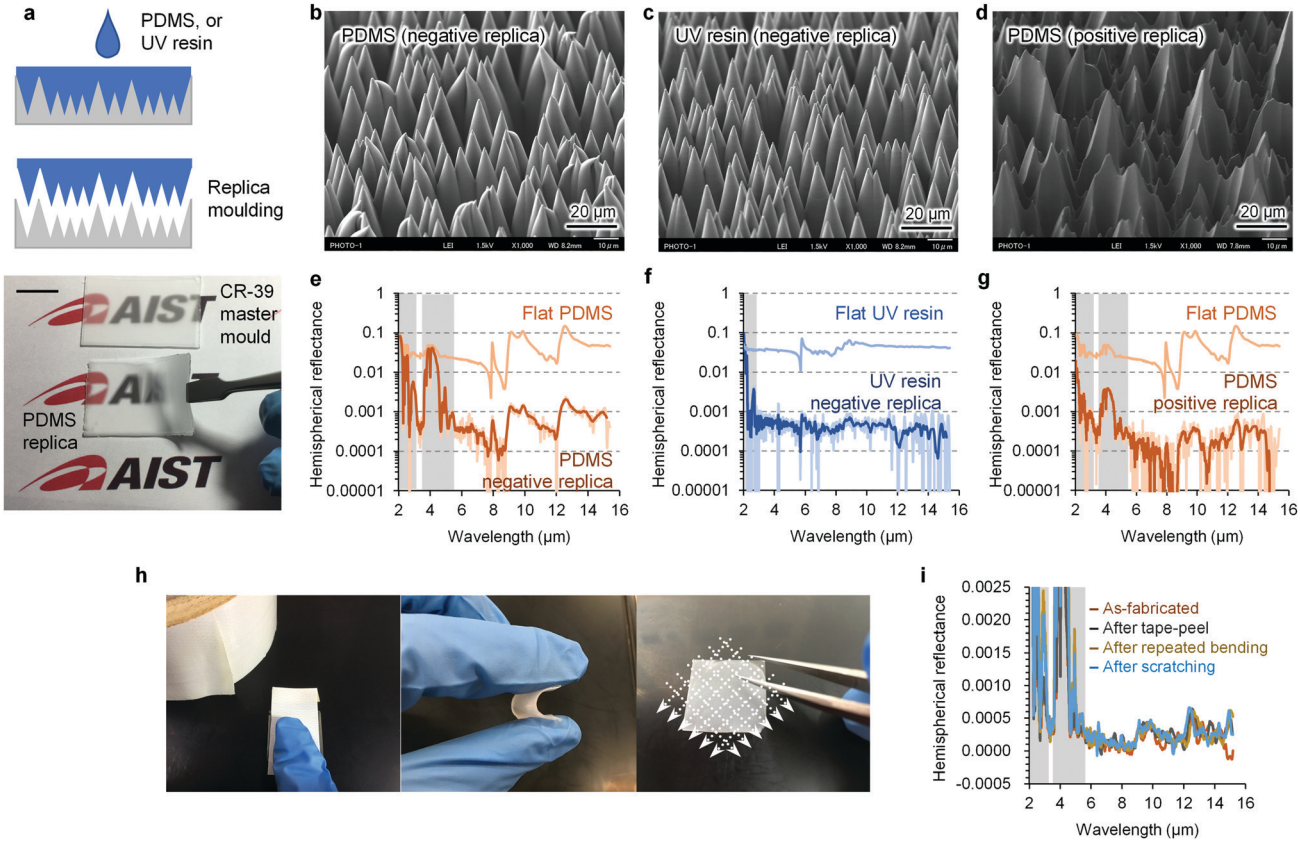

Fig. 3 Characterization of elastomeric micro-cavity blackbody sheets. (a) Fabrication procedure of an elastomeric micro-cavity sheet *via* replica moulding. Scale bar, 10 mm. (b–d) SEM images of the micro-cavity blackbody sheets of PDMS negative (b) and positive (d) replicas, and UV resin negative replica (c). (e–g) Corresponding hemispherical reflectance of the elastomeric micro-cavity sheets, accompanied with the Fresnel reflectance of untextured (flat) elastomers. The dark solid line for each embossed elastomer denotes moving average of 20 neighbouring plots. (h) Durability test of the PDMS micro-cavity positive replica: tape-pulling (left), repeated bending (centre) and scratching (right). (i) Any mechanical perturbation here hardly changed the ultralow reflectance. Grey bands in the reflectance spectra denote the wavelengths in which the embossed elastomers become transmissive.

with or better than the best case of CNT forests[11,29] at thermal infrared wavelengths (8–14 μm). Note that a PDMS sheet was transmissive at 3.5–6 μm (grey band in Fig. 3e), confirmed by reflectance measurement with a metal plate placed behind the sheet (see Experimental section). Instead of PDMS, common ultraviolet (UV) curing resin was also applicable for replication (Fig. 3c). The UV resin replica exhibited better spectral flatness at wider wavelengths of 3–15 μm (Fig. 3f). The reflectance (<0.001) was comparably low to that of the PDMS replica, while the UV resin replica had less elasticity, which sometimes caused difficulty in peeling-off from the master mould.

Other than elastomers, electroforming[15] provided metal replicas, serving as more rigid stamp moulds than the CR-39 master mould (Fig. S3, ESI†). This stamp mould produced a positive replica with the same texture as the master mould (pit-type cavity). Notably, the positive replica from PDMS (Fig. 3d) exhibited a reflectance of $\lesssim 0.0005$ over the entire mid-infrared regime (6–15 μm, Fig. 3g), which was a better performance than that of the spike-type cavity (Fig. 3e). Numerical simulation suggested that both types of micro-cavities (spike and pit) were expected to show comparably low reflectance (Fig. S1b and c, ESI†). The experimental discrepancy is probably attributable to the PDMS spike's tendency of pairing – adhesion between neighbouring spikes (Fig. 3b), leading to partial failure of antireflection. The above discussion supports that the nanometric precision of the micro-cavities is essential for perfect absorption.

The advantage of elastomeric sheets is high resilience against direct touch and deformation. The following discussion focuses on the positive (pit-type) PDMS replicas from a usability and customizability point-of-view. In contrast to CNT forests, tape pulling, repeated bending or scratching on our PDMS micro-cavities hardly changed their ultralow reflectance within <0.0005 (see Experimental section, Fig. 3h and i). Markedly, the scratch-proof nature is unmatched among existing planar near-perfect blackbodies. The tape-pulling resistance enables instant dust removal or facile film protection. Such resilience, thereby, promises easy handling without special care. Ultrasonic cleaning, however, often resulted in increased reflectance of the PDMS blackbody sheet, presumably owing to the water capillary force, causing the pairing of textures. Nevertheless, the degraded texture was restored to exhibit the original performance (Fig. S4a, ESI†) by exposure to sodium dodecyl sulphate

solution and following heptane rinse, whose surface activity would recuperate the pairing (see ESI†).[48] Meanwhile, immersion into liquid nitrogen made little influence on their ultralow reflectance, regardless of temporary deep frosting after liquid nitrogen evaporation (Fig. S4b and d, ESI†). The PDMS blackbody sheets had heat resistance, as well, against ~190 °C (Fig. S4c and d, ESI†). The low reflectance was maintained over an entire year of storage at ambient conditions, although further long-term stability is under investigation.

Our elastomeric blackbody sheets would flexibly conform to a surface inside a consumer device. Infrared optics in a thermal imager is one of the most appropriate application areas. The image contrast and the temperature indication accuracy of thermal imagers often deteriorate due to stray infrared radiation, which can hardly be corrected by pre-calibration because the source of stray radiation varies under each situation.[23] Here we demonstrated that the PDMS blackbody sheet unprecedentedly eliminated stray infrared radiation (see Experimental section, Fig. 4a); any thermal ghost reflection due to a nearby high-temperature object was hardly recognized on our blackbody sheet in a thermographic image (Fig. 4b). Therefore our blackbody sheets will offer the precision thermal imaging, including for FTIR microscopy,[22] fever screening,[25] remote sensing of the environment[23] and infrared telescopy to detect highly red-shifted early universe stars or exoplanet atmospheres.[24] Our blackbody sheets would also serve as a planar standard radiator, affording to calibrate thermal imagers. Therein, the emissivity correction can be the smallest ever ($\Delta\varepsilon/\varepsilon$ = 0.001, conservatively), corresponding to the temperature uncertainty $\Delta T < 0.05$ °C at ambient temperature (~23 °C). More practically, their use as blackbody tapes, which turn an arbitrary surface into near-unity emissivity, would enable the most accurate radiation thermometry (note that thermal conductivity of blackbody sheets is also key issue for the precision blackbody applications: see ESI†). In another viewpoint, the highest emissivity of our PDMS blackbody sheets would maximize thermal radiation for passive cooling[8–10,26,27] as well.

For such thermal infrared applications, we can use the PDMS blackbody sheet just as it is, regardless of its visible transparency. Yet visually, very black materials are still aesthetically pleasing and functional. We demonstrated the pre-addition of carbon black filler into a PDMS blackbody sheet (see Experimental section, Fig. 5a). The resultant sheet exhibited a remarkably reduced reflectance of 0.003–0.005 at wavelengths of 250 nm–6 μm (Fig. 5b). The ultralow reflectance of ≲0.001 was maintained

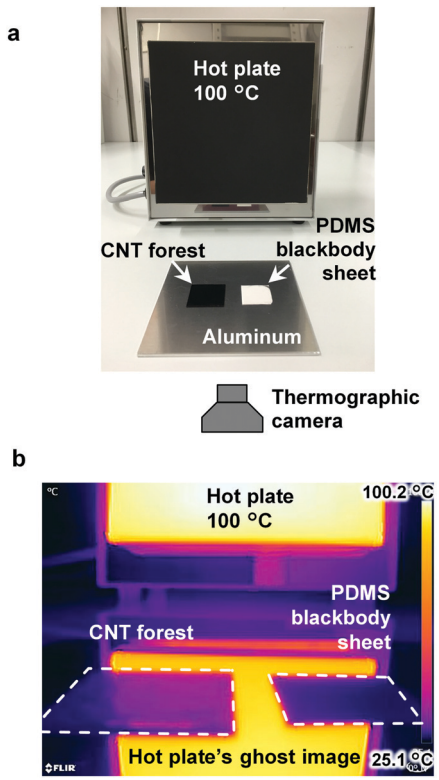

Fig. 4 Application of elastomeric micro-cavity blackbody sheet. (a) Demonstration setup for deep reduction of stray infrared radiation in thermography. (b) The obtained thermographic image in pseudo colour. Any thermal ghost reflection due to the high-temperature object (hot plate) was unrecognized on the micro-cavity blackbody sheet, while the clear-contrast thermal ghost was recognized on a 40 μm-long CNT forest.

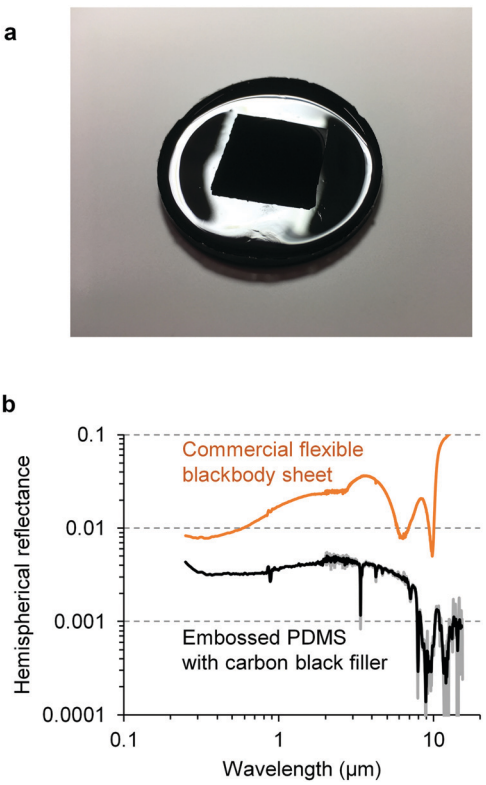

Fig. 5 Micro-cavity blackbody sheet from a visibly blackened elastomer. (a) The PDMS blackbody sheet with carbon black filler placed on an untextured PDMS with carbon black. Any reflected glare was unrecognized on the blackbody sheet (centre squared area). (b) Hemispherical reflectance the PDMS blackbody sheet with carbon black filler (black solid line) in comparison with a commercial flexible blackbody sheet of Acktar Metal Velvet (orange solid line). The grey solid line denotes the obtained data at mid-infrared wavelengths, whereas the corresponding black solid line denotes moving average of 20 neighbouring plots.

at >8 μm in wavelength. According to the numerical simulation, further reduction of the reflectance into <0.001 would be expected (Fig. S1d, ESI†); indeed, another type of replica from electroformed nickel experimentally exhibited the expected reflectance of <0.002 at wavelengths of 250–570 nm (Fig. S3, ESI†). In this study, carbon black filler was mixed *via* manual stirring into PDMS prepolymer, and, therefore, may easily form aggregates of the size larger than the visible wavelength. Incident light can suffer diffuse reflection at the aggregates, resulting in unwanted photon escape from the micro-cavities. The key challenge would be a homogeneous dispersion of the black filler. Nevertheless, at this moment, our blackbody sheet exhibited the lowest-ever reflectance among flexible planar black absorbers,[5,38] including a commercial product of Acktar Metal Velvet[49] (Fig. 5b).

Conclusions

In summary, we have developed the elastomeric perfect blackbody sheets exhibiting an exceptionally low reflectance ($\lesssim$0.0005) over the entire mid-infrared wavelengths (6–15 μm), while maintaining high mechanical resilience. This performance stems from nano-precision micro-cavities fabricated *via* simple two step procedures of swift heavy ion manufacturing and replica moulding. This promising blackbody sheet affords the unprecedented management of thermal radiation. As an example, we demonstrated the perfect elimination of thermal ghost reflection in thermography, which would offer clear and accurate thermal imaging for fever screening, Earth observation and so on. This performance has not yet been reached by CNT forests as well as other nanophotonic absorbers. Aligned CNTs are still attractive in electronics, thermodynamics or mechanics. Sparse CNT forests as perfect absorbers, however, would be under the risk of mechanical damage when exposed to the open environment, leading to not only degraded absorptance but also emission of airborne fibre-shaped nanomaterials. It still remains elusive whether exposure to long-fibre CNTs causes malignant lung tumours with long latency.[50] In contrast, our elastomeric blackbody sheets cause no inhalation or contamination risk from nano-aerosols. Our perfect blackbody sheets would open up wider applications in the general public, from dark-level reduction to light management/harvesting.

Experimental section

Materials

CR-39 substrates of BARYOTRAK were purchased from Fukuvi Chemical Industry Co., Ltd, Japan. Sodium hydroxide solution was purchased from FUJIFILM Wako Pure Chemical Corporation, Japan. UV curing resin of Uni Solar Soft, containing urethane acrylate, triethylene glycol dimethacrylate and 2-hydroxy-2-methyl-1-phenyl-1-propanone was purchased from UNITEC Co., Ltd, Japan. PDMS for high-precision mould making of SIM-360 prepolymer and CAT-360 curing agent were purchased from Shin-Etsu Chemical Co., Ltd, Japan. Acetylene carbon black (50% compressed, averaged particle size 0.042 μm) was purchased from Strem Chemicals, Inc., USA. For comparison purposes, a multiwall carbon nanotube forest of 40 μm length was grown on nickel substrate by chemical vapour deposition, conducted by Microphase Co., Ltd, Japan. A commercially available blackbody sheet of high flexibility (Metal Velvet, Acktar Ltd, Israel) was also purchased for comparison.

Preparation of micro-cavity template

To fabricate the micro-cavity template, we conducted swift heavy ion manufacturing. CR-39 plates of 0.8 mm thickness were cut into 100 mm × 100 mm size, and then irradiated by heavy ion beam from an azimuthally varying field cyclotron at the TIARA, National Institutes for Quantum and Radiological Science and Technology (QST). The sample chamber was kept at a vacuum of 10^{-3} Pa during the irradiation to avoid excess energy loss of the ion beam. According to the Stopping and Range of Ions in Matter (SRIM)[51] calculation, we chose a 260 MeV neon ion beam; it has a substantial penetration depth of >300 μm, and damage density per unit path length (linear energy transfer: LET) of ~450 keV μm^{-1} in the CR-39, yielding etch pits with sufficient depth (several tens of μm) and an aspect ratio of more than 5 (ref. 47). The irradiation density was 1×10^6 ions cm^{-2}. After the irradiation, the 100 mm × 100 mm CR-39 substrate was cut into several smaller pieces and etched in 6.4 mol L^{-1} NaOH solution at 70 °C for around 7 h to ensure that etch pits filled the entire surface of the substrate. The average pit opening diameter was ~11 μm.

Fabrication of elastomeric perfect blackbody sheets

Elastomeric perfect blackbody sheets were fabricated by replica moulding[37] of a template from the microtextured CR-39. PDMS prepolymer (SIM-360, Shin-Etsu) was mixed with the curing agent (CAT-360) at a concentration of 10 : 1 and degassed in a vacuum desiccator. The PDMS prepolymer was then poured on the micro-cavity template to a thickness of ~1 mm and degassed again. After overnight curing at room temperature, the replica of PDMS was peeled off from the template. The replicas from pure PDMS were perfectly absorptive in the mid-infrared but also visibly transmissive. To extend the spectral range of near-perfect absorption to the visible regime, acetylene carbon black of 5% by weight was pre-added in the PDMS prepolymer and manually mixed to be used in replica moulding.

For UV curing resin replication, the procedure was similar to that for PDMS except for the material and curing process. A UV lamp of 365 nm in wavelength, 9 W in power was irradiated to UV curing resin poured on the template for approximately five minutes.

These replication processes can be repeatedly applied with a single micro-cavity template.

Surface characterization

The sample surface morphology was observed with an SEM of JSM-7400F from JEOL Ltd, Japan. The electron acceleration voltage was 1.5 kV. To avoid electronic charge up of the insulative sample, a conductive layer of thin (~5 nm) platinum was coated prior to observation.

Optical characterization

The spectral reflectance of the samples was measured using spectrometers. For wavelengths of 2–15 μm, an FT/IR-6300typeA FTIR spectrometer from JASCO Corporation, Japan, was used with a 3 inch diffusive-gold integrating sphere and a liquid-nitrogen-cooled mercury cadmium telluride detector (IntegratIR, PIKE Technologies, USA). Sample hemispherical reflectance was determined in comparison to a reference reflectance standard of ~0.9 reflectance level (Infragold, Labsphere, USA). The measurement was conducted at 12°/d geometry, that is, light incident angle was 12°, and the reflectance was integrated over all hemispherical viewing directions including both specular and diffusive components. At least two samples were measured for each type of blackbody sheet, and the results were well reproduced. Exceptionally, the data at the wavelength band where the samples became transmissive were highly dependent on the sample bottom conditions (see also Relation between reflectance and absorptance).

For UV-NIR, a spectrophotometer (LAMBDA 900 with a 6 inch integrating sphere from PerkinElmer, Inc., USA) and a Spectralon reflectance standard of 0.99 reflectance level from Labsphere, Inc., USA were used. The measurement was conducted at 8°/d geometry.

The measurement of ultralow reflectance requires special care; we conducted the measurement according to the guide of ref. 28. In particular, the measurement system's (1) throughput, (2) baseline signal and (3) response linearity had to be considered in detail (see ESI†).

Relation between reflectance and absorptance

To confirm whether the reflectance R is correlated with the absorptance A, as $A = 1 - R$, an opaque material, such as a metal plate, was placed behind the sample during the reflectance measurement. Increase of the reflectance when the metal plate was placed behind implies that the sample is transmissive; otherwise, the sample is absorptive (opaque). Our microtextured polymer substrate or elastomer sheet of substantial optical thickness (physically ~1 mm) was confirmed to be opaque at long-wavelength infrared from 6–15 μm. At shorter wavelengths, the samples, particularly PDMS micro-cavity sheet, had a transmissive wavelength band as shown in Fig. 3e–g and i (grey band).

Durability test

Mechanical durability of the PDMS blackbody sheet was tested by applying an adhesive tape (packing tape) and its subsequent peeling-off; bending repeatedly (for 500 times, bending radius of ~5 mm); and scratching with a sharp tweezer in 3 mm grid spacing over the entire sample. After each testing procedure, the spectral reflectance of the sample was measured again and compared with that prior to the test.

Thermographic demonstration

To demonstrate deep suppression of stray thermal infrared, a PDMS blackbody sheet was placed in front of a high-temperature object (a hot plate) and visualized by a thermal imager. The hot plate (DSI-180, AS ONE Corporation, Japan) was set to be 100 °C. The thermal imager (FLIR One Pro, FLIR Systems, Inc., USA) has an uncooled microbolometer array sensor for the long-wave infrared (8–14 μm). The emissivity setting of the thermal imager was chosen to be 1.0. For comparison, a multiwall CNT forest of 40 μm long was placed next to the PDMS blackbody sheet. Both samples were in equilibrium with the ambient condition (23 °C in temperature).

Conflicts of interest

Corresponding author (K. A.) is an inventor on a patent application related to this work, filed by National Institute of Advanced Industrial Science and Technology, Japan (patent application number: PCT/JP2018/017949). The other authors declare no competing financial interests.

Acknowledgements

This work was supported by JSPS KAKENHI Grant Number JP18K11940. The ion beam irradiation experiment was conducted at Takasaki Ion Accelerators for Advanced Radiation Application (TIARA) of National Institutes for Quantum and Radiological Science and Technology (QST), Takasaki, Japan, which was supported by the Inter-University Program for the Joint Use of JAEA/QST Facilities (proposal no. 18004). Scanning electron microscope (SEM) imaging was conducted with support from Tsukuba Innovation Arena for Nanotechnology (TIA-nano) of National Institute of Advanced Industrial Science and Technology (AIST), Japan.

References

1 Y.-F. Huang, S. Chattopadhyay, Y.-J. Jen, C.-Y. Peng, T.-A. Liu, Y.-K. Hsu, C.-L. Pan, H.-C. Lo, C.-H. Hsu, Y.-H. Chang, C.-S. Lee, K.-H. Chen and L.-C. Chen, *Nat. Nanotechnol.*, 2007, **2**, 770–774.
2 Z.-P. Yang, L. Ci, J. A. Bur, S.-Y. Lin and P. M. Ajayan, *Nano Lett.*, 2008, **8**, 446–451.
3 K. Mizuno, J. Ishii, H. Kishida, Y. Hayamizu, S. Yasuda, D. N. Futaba, M. Yumura and K. Hata, *Proc. Natl. Acad. Sci. U. S. A.*, 2009, **106**, 6044–6047.
4 R. J. C. Brown, P. J. Brewer and M. J. T. Milton, *J. Mater. Chem.*, 2002, **12**, 2749–2754.
5 M. K. Hedayati, M. Javaherirahim, B. Mozooni, R. Abdelaziz, A. Tavassolizadeh, V. S. K. Chakravadhanula, V. Zaporojtchenko, T. Strunkus, F. Faupel and M. Elbahri, *Adv. Mater.*, 2011, **23**, 5410–5414.
6 M. J. Persky, *Rev. Sci. Instrum.*, 1999, **70**, 2193–2217.
7 E. Theocharous, C. J. Chunnilall, R. Mole, D. Gibbs, N. Fox, N. Shang, G. Howlett, B. Jensen, R. Taylor, J. R. Reveles, O. B. Harris and N. Ahmed, *Opt. Express*, 2014, **22**, 7290–7307.
8 L. Zhu, A. P. Raman and S. Fan, *Proc. Natl. Acad. Sci. U. S. A.*, 2015, **112**, 12282–12287.

9 Y. Zhai, Y. Ma, S. N. David, D. Zhao, R. Lou, G. Tan, R. Yang and X. Yin, *Science*, 2017, **355**, 1062–1066.
10 J.-L. Kou, Z. Jurado, Z. Chen, S. Fan and A. J. Minnich, *ACS Photonics*, 2017, **4**, 626–630.
11 J. Lehman, A. Sanders, L. Hanssen, B. Wilthan, J. Zeng and C. Jensen, *Nano Lett.*, 2010, **10**, 3261–3266.
12 J. Lehman, E. Theocharous, G. Eppeldauer and C. Pannell, *Meas. Sci. Technol.*, 2003, **14**, 916–922.
13 A. Lenert, D. M. Bierman, Y. Nam, W. R. Chan, I. Celanović, M. Soljačić and E. N. Wang, *Nat. Nanotechnol.*, 2014, **9**, 126–130.
14 N. Selvakumar, S. B. Krupanidhi and H. C. Barshilia, *Adv. Mater.*, 2014, **26**, 2552–2557.
15 P. Li, B. Liu, Y. Ni, K. K. Liew, J. Sze, S. Chen and S. Shen, *Adv. Mater.*, 2015, **27**, 4585–4591.
16 H. Savin, P. Repo, G. von Gastrow, P. Ortega, E. Calle, M. Garín and R. Alcubilla, *Nat. Nanotechnol.*, 2015, **10**, 624–628.
17 Z. Liu, X. Liu, S. Huang, P. Pan, J. Chen, G. Liu and G. Gu, *ACS Appl. Mater. Interfaces*, 2015, **7**, 4962–4968.
18 L. Zhou, Y. Tan, D. Ji, B. Zhu, P. Zhang, J. Xu, Q. Gan, Z. Yu and J. Zhu, *Sci. Adv.*, 2016, **2**, e1501227.
19 C. Chen, Y. Li, J. Song, Z. Yang, Y. Kuang, E. Hitz, C. Jia, A. Gong, F. Jiang, J. Y. Zhu, B. Yang, J. Xie and L. Hu, *Adv. Mater.*, 2017, **29**, 1701756.
20 Z. Yin, H. Wang, M. Jian, Y. Li, K. Xia, M. Zhang, C. Wang, Q. Wang, M. Ma, Q.-S. Zheng and Y. Zhang, *ACS Appl. Mater. Interfaces*, 2017, **9**, 28596–28603.
21 C. Ng, L. W. Yap, A. Roberts, W. Cheng and D. E. Gómez, *Adv. Funct. Mater.*, 2017, **27**, 1604080.
22 A. S. Tagg, M. Sapp, J. P. Harrison and J. J. Ojeda, *Anal. Chem.*, 2015, **87**, 6032–6040.
23 M. Montanaro, A. Gerace and S. Rohrbach, *Appl. Opt.*, 2015, **54**, 3963–3978.
24 M. Wells, J.-W. Pel, A. Glasse, G. S. Wright, G. Aitink-Kroes, R. Azzollini, S. Beard, B. R. Brandl, A. Gallie, V. C. Geers, A. M. Glauser, P. Hastings, T. Henning, R. Jager, K. Justtanont, B. Kruizinga, F. Lahuis, D. Lee, I. Martinez-Delgado, J. R. Martínez-Galarza, M. Meijers, J. E. Morrison, F. Müller, T. Nakos, B. O'Sullivan, A. Oudenhuysen, P. Parr-Burman, E. Pauwels, R.-R. Rohloff, E. Schmalzl, J. Sykes, M. P. Thelen, E. F. van Dishoeck, B. Vandenbussche, L. B. Venema, H. Visser, L. B. F. M. Waters and D. Wright, *Publ. Astron. Soc. Pac.*, 2015, **127**, 646–664.
25 P. Ghassemi, T. J. Pfefer, J. P. Casamento, R. Simpson and Q. Wang, *PLoS One*, 2018, **13**, e0203302.
26 L. Zhu, A. Raman, K. X. Wang, M. A. Anoma and S. Fan, *Optica*, 2014, **1**, 32–38.
27 A. P. Raman, M. A. Anoma, L. Zhu, E. Rephaeli and S. Fan, *Nature*, 2014, **515**, 540–544.
28 J. Lehman, C. Yung, N. Tomlin, D. Conklin and M. Stephens, *Appl. Phys. Rev.*, 2018, **5**, 011103.
29 Z.-P. Yang, M.-L. Hsieh, J. A. Bur, L. Ci, L. M. Hanssen, B. Wilthan, P. M. Ajayan and S.-Y. Lin, *Appl. Opt.*, 2011, **50**, 1850–1855.
30 P. Yu, L. V. Besteiro, Y. Huang, J. Wu, L. Fu, H. H. Tan, C. Jagadish, G. P. Wiederrecht, A. O. Govorov and Z. Wang, *Adv. Opt. Mater.*, 2019, **7**, 1800995.
31 N. Liu, M. Mesch, T. Weiss, M. Hentschel and H. Giessen, *Nano Lett.*, 2010, **10**, 2342–2348.
32 A. Moreau, C. Ciracì, J. J. Mock, R. T. Hill, Q. Wang, B. J. Wiley, A. Chilkoti and D. R. Smith, *Nature*, 2012, **492**, 86–89.
33 J. Ishii, M. Kobayashi and F. Sakuma, *Metrologia*, 1998, **35**, 175–180.
34 K. Amemiya, D. Fukuda, T. Numata, M. Tanabe and Y. Ichino, *Appl. Opt.*, 2012, **51**, 6917–6925.
35 A. Deinega, I. Valuev, B. Potapkin and Y. Lozovik, *J. Opt. Soc. Am. A*, 2011, **28**, 770–777.
36 K. Amemiya, H. Koshikawa, T. Yamaki, Y. Maekawa, H. Shitomi, T. Numata, K. Kinoshita, M. Tanabe and D. Fukuda, *Nucl. Instrum. Methods Phys. Res., Sect. B*, 2015, **356–357**, 154–159.
37 D. Qin, Y. Xia and G. M. Whitesides, *Nat. Protoc.*, 2010, **5**, 491–502.
38 T. Ji, Y. Wang, Y. Cui, Y. Lin, Y. Hao and D. Li, *Mater. Today Energy*, 2017, **5**, 181–186.
39 H. Mukaibo, L. P. Horne, D. Park and C. R. Martin, *Small*, 2009, **5**, 2474–2479.
40 N. Stutzmann, T. A. Tervoort, C. W. M. Bastiaansen, K. Feldman and P. Smith, *Adv. Mater.*, 2000, **12**, 557–562.
41 N. Yasuda, M. Yamamoto, K. Amemiya, H. Takahashi, A. Kyan and K. Ogura, *Radiat. Meas.*, 1999, **31**, 203–208.
42 B. Wu, A. Kumar and S. Pamarthy, *J. Appl. Phys.*, 2010, **108**, 051101.
43 D. Dornfeld, S. Min and Y. Takeuchi, *CIRP Ann.*, 2006, **55**, 745–768.
44 N. Yasuda, K. Uchikawa, K. Amemiya, N. Watanabe, H. Takahashi, M. Nakazawa, M. Yamamoto and K. Ogura, *Radiat. Meas.*, 2001, **34**, 45–49.
45 P. Y. Apel, I. V. Blonskaya, N. E. Lizunov, K. Olejniczak, O. L. Orelovitch, M. E. Toimil-Molares and C. Trautmann, *Small*, 2018, **14**, 1703327.
46 B. G. Cartwright, E. K. Shirk and P. B. Price, *Nucl. Instrum. Methods*, 1978, **153**, 457–460.
47 S. Kodaira, N. Yasuda, H. Kawashima, M. Kurano, S. Naka, S. Ota, Y. Ideguchi, N. Hasebe and K. Ogura, *Radiat. Meas.*, 2011, **46**, 1782–1785.
48 E. Delamarche, H. Schmid, B. Michel and H. Biebuyck, *Adv. Mater.*, 1997, **9**, 741–746.
49 Acktar Ltd., http://www.acktar.com, accessed: March, 2019.
50 T. Chernova, F. A. Murphy, S. Galavotti, X. Sun, I. R. Powley, S. Grosso, A. Schinwald, J. Zacarias-Cabeza, K. M. Dudek, D. Dinsdale, J. Le Quesne, J. Bennett, A. Nakas, P. Greaves, C. A. Poland, K. Donaldson, M. Bushell, A. E. Willis and M. MacFarlane, *Curr. Biol.*, 2017, **27**, 3302–3314.
51 J. F. Ziegler, M. D. Ziegler and J. P. Biersack, *Nucl. Instrum. Methods Phys. Res., Sect. B*, 2010, **268**, 1818–1823.